batteries

MDPI

*Article*

# Influence of High Temperature on Cycling and Calendar Degradation of Lithium-Ion Batteries with Thermal Changes

**Ruiheng Wang [1] and Bing Xue [2,*]**

[1] School of Safety Science and Engineering, Changzhou University, Changzhou 213164, China
[2] Jiangsu Key Laboratory of Advanced Catalytic Materials and Technology, School of Petrochemical Engineering, Changzhou University, Changzhou 213164, China
* Correspondence: xuebing@cczu.edu.cn

**Abstract**

The aging mechanism and safety revolution of lithium-ion batteries (LIBs) are always influenced by the working temperature. The degradation path and thermal characteristics of LIBs at high temperature were investigated both from the aspect of cycle aging and calendar aging in this study. High temperature (55 °C) with temperature rate, cycle number, calendar time, and charging/discharging rate were taken into consideration to validate the battery performance under dynamic operating conditions. The basic electrochemical index, including capacity loss, internal resistance growth, and incremental capacity curve (IC curve) of LIBs, was first analyzed. Then, capacity loss and internal resistance growth were calculated both under cycling and calendar conditions with high temperature. Thermal characteristics were further analyzed by entropy change, enthalpy change, and temperature rate during the high-temperature cycling. Moreover, adiabatic thermal experimental results under 0% state of charge (SOC) were also conducted for further safety analysis. A non-monotonic calendar-aging maximum near 75% SOC and a rate-dependent degradation minimum at intermediate rates were identified. The aging and calendar laws of LIBs at high temperature and high rate were then concluded as reference to support the usage management and storage strategies of LIBs.

**Keywords:** lithium-ion batteries; high temperature; battery degradation; calendar aging; thermal characteristics

## 1. Introduction

Electric vehicles (EVs), energy storage systems (ESSs), and other transportation applications usually employ lithium-ion batteries (LIBs) as power sources, which operate under complex conditions [1,2]. Owing to the electrochemical characteristics of LIBs, the charge or discharge current directly affects the cycle life, calendar life, and safety of LIBs [3,4]. The ambient temperature of an operating battery is another critical factor affecting lithium-ion activation, especially at relatively high temperatures (>45 °C) or low temperatures (<0 °C) [5–8]. Hence, a battery management system (BMS) is designed to efficiently monitor states, manage lifetime, and ensure LIB safety in these applications.

Capacity loss and internal resistance growth are considered main indicators of battery degradation [9,10]. Estimation of state of charge (SOC), state of health (SOH), and state of safety (SOS) has been studied in recent years [2,11]. The incremental capacity (IC) curve describes capacity change per unit voltage during charging and discharging. It reveals changes in internal electrochemical reactions and thus reflects variations in loss of active material (LAM) and loss of lithium inventory (LLI) [12]. Previous studies showed that

Check for updates

Academic Editors: Odne S. Burheim and Pascal Venet

Received: 25 August 2026
Revised: 14 October 2026
Accepted: 31 October 2026
Published: 17 November 2026

**Copyright:** © 2026 by the authors. Licensee MDPI, Basel, Switzerland. This article is an open access article distributed under the terms and conditions of the Creative Commons Attribution (CC BY) license.

aging increases side reaction products, such as lithium plating or gas. These products inevitably affect electrochemical reactions and cause key LIB parameters to degrade over the lifetime [13,14]. To understand calendar aging behavior and evaluate whether performance still meets requirements after long-term storage, it is necessary to analyze calendar aging performance and degradation behavior [6,15].

Taking temperature into consideration, researchers have also proposed related work on aging mechanism and safety revolution of LIBs at high temperature or high-temperature conditions [16,17]. Aging path and degradation characteristics at high temperature may influence degradation during battery cycling [18]. Battery cycling also needs to be considered and combined with temperature conditions to illustrate long-term characteristics [19,20]. However, these studies mainly address individual aging paths; the coupled comparison under identical high-temperature conditions remains to be improved. Since large current would bring severe polarization and solid electrolyte interphase (SEI) growth to a battery [21–23], the charging or discharging rate at high temperature is also a vital research direction to analyze the dynamic energy supply ability of an LIB [24–26]. Chemical reactions during operation cause the rearrangement of atoms and ions, inducing entropy change inside LIBs, which is accompanied by energy absorption and release, leading to temperature rise. Hence, thermodynamic parameters such as entropy heat coefficient, entropy change, and enthalpy change are important indicators for the heat generation calculation and thermal safety analysis after the high-temperature cycling aging of lithium-ion batteries [27–30].

This paper explored the degradation evolution, calendar lifetime, and safety characteristics of LIBs at high temperature. High temperature (55 °C) with temperature rate, cycle number, calendar life, and charging/discharging rate are taken into consideration to test the battery performance under dynamic operating conditions. Based on experimental results, the trends of capacity loss, internal resistance growth, and incremental capacity curve (IC curve) were analyzed to illustrate the basic electrochemical characteristics of LIBs. The aging laws both under cycling and calendar conditions are provided for LIB usage and storage under high temperature. Thermal characteristics were analyzed by entropy change, enthalpy change, and temperature rate during high-temperature cycling. Moreover, adiabatic thermal experimental results under 0% SOC were also conducted for further safety analysis. Several evolution rules of degradation and safety were concluded as reference to support further design of thermal management strategies or lifetime estimation. Unlike previous studies that focused on isolated aging modes, this work establishes a unified high-temperature experimental matrix for the same commercial 18650 cell, covering cycling aging, calendar aging, rate-dependent aging, IC evolution, thermodynamic parameters, and thermal stability.

## 2. Battery Experiment System

### *2.1. Cell Information*

This paper used the cylindrical 18650 commercial power battery (Sony US18650VTC6) as the research object, and the parameters are shown in Table 1. The electrochemical characteristics, cycling characteristics, heat generation characteristics, and safety characteristics were investigated in the following.

**Table 1.** The parameter information of battery cell sample.

| Type | Value |
|---|---|
| positive material type | Nickel Cobalt Manganese (NCM) |
| rated capacity/voltage | 3000 mAh, 3.6 V |
| max charging voltage | 4.20 ± 0.05 V |
| cut-off voltage | 2.50 V |
| max discharging current | 30 A |
| diameter/height | 18 mm/65 mm |
| weight | 45.1 ± 1.5 g |

### *2.2. Experiment Conditions*

The experimental equipment in this study includes a battery tester, a chamber, an accelerating rate calorimeter (ARC), and a data acquisition unit, as shown in Table 2.

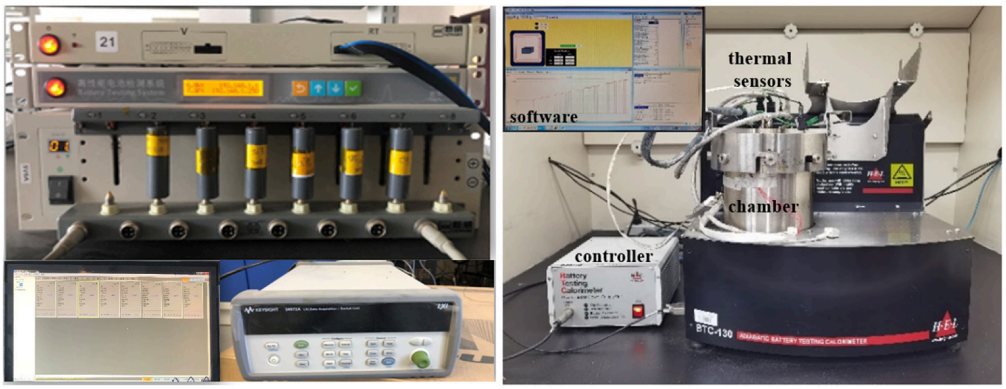
**Table 2.** Summary of all experimental equipment used in this study.

| Equipment | Model | Manufacturer |
|---|---|---|
| high-precision battery tester | CT-4008-5V12A-DB | Neware, Dongguan, China |
| temperature chamber | ETH-1000 | Lijia, Dongguan, China |
| data acquisition unit | CA-4008-1U-VT | Neware, Dongguan, China |
| accelerating rate calorimeter | BTC-130 | HEL, London, UK |

(1) Battery cycle testing system

The battery cycle testing system consists of three components as follows:

a. a high-precision battery tester (CT-4008-5V12A-DB) with ±0.1% voltage/current accuracy, including master unit and eight channels supporting 5 V, 12 A simultaneous charging/discharging, as shown in Figure 1a;
b. a data acquisition unit (CA-4008-1U-VT) for battery charging/discharging data collection, providing ±0.1 °C measurement accuracy;
c. a PC and its control software.




(**a**) (**b**)

**Figure 1.** Battery performance test system: (**a**) battery cycle tester, (**b**) accelerating rate calorimeter.

(2) Battery safety testing system

The accelerating rate calorimeter (ARC) is widely used to study the thermal characteristics and safety of LIBs. This study employed an ARC HEL BTC-130 with a maximum tracking temperature of 500 °C, a maximum vessel pressure of 4 bar, and a high-stability temperature control of 0.1% accuracy, to construct adiabatic conditions by heat compensation, as shown in Figure 1b. The thermal characteristics of LIB samples with varying

aging levels under high temperature were investigated to explore the evolution of the safety performance.

### 2.3. Experiment Setups

(1) High-temperature cycling aging experiment

Two experimental sets were designed to separate cycle-number and temperature effects. In the cycle-number-dependent set, eight groups of cells were aged at 55 °C under continuous 3C charge/discharge cycling for 0, 25, 50, 75, 100, 125, 150, and 200 cycles, with three cells per group (24 cells in total). In the temperature-dependent set, cells were cycled at a fixed cycle number of 200 cycles at 10 °C, 25 °C, 35 °C, 45 °C, and 55 °C, with one cell per temperature (5 cells in total). All cycling adopted constant current-constant voltage (CC-CV) charging and constant current discharging. The charge cutoff voltage was 4.2 V with a cutoff current of 0.05C (0.15 A), and the discharge cutoff voltage was 2.5 V. A 30 min rest period was inserted between charge and discharge steps to eliminate polarization and voltage relaxation. The detailed grouping is listed in Table 3.

**Table 3.** Experimental setup of temperature on battery aging.

**(a) Different cyclings at high temperature**

| Type | Charge Rate | Discharge Rate | Charge/Discharge Cutoff Voltage | Temperature | Cycles | Samples |
|---|---|---|---|---|---|---|
| 1 | 3C | 3C | 4.2 V–2.5 V | 55 °C | 0 | 3 |
| 2 | 3C | 3C | 4.2 V–2.5 V | 55 °C | 25 | 3 |
| 3 | 3C | 3C | 4.2 V–2.5 V | 55 °C | 50 | 3 |
| 4 | 3C | 3C | 4.2 V–2.5 V | 55 °C | 75 | 3 |
| 5 | 3C | 3C | 4.2 V–2.5 V | 55 °C | 100 | 3 |
| 6 | 3C | 3C | 4.2 V–2.5 V | 55 °C | 125 | 3 |
| 7 | 3C | 3C | 4.2 V–2.5 V | 55 °C | 150 | 3 |
| 8 | 3C | 3C | 4.2 V–2.5 V | 55 °C | 200 | 3 |

**(b) Aging comparison under different temperatures**

| Type | Charge Rate | Discharge Rate | Charge/Discharge Cutoff Voltage | Temperature | Cycles | Samples |
|---|---|---|---|---|---|---|
| 1 | 3C | 3C | 4.2 V–2.5 V | 10 °C | 200 | 1 |
| 2 | 3C | 3C | 4.2 V–2.5 V | 25 °C | 200 | 1 |
| 3 | 3C | 3C | 4.2 V–2.5 V | 35 °C | 200 | 1 |
| 4 | 3C | 3C | 4.2 V–2.5 V | 45 °C | 200 | 1 |
| 5 | 3C | 3C | 4.2 V–2.5 V | 55 °C | 200 | 1 |

(2) High-temperature calendar aging experiment

To investigate the calendar aging behavior of LIBs under high temperature, the calendar aging experiment was designed as shown in Table 4. During calendar aging, ten batteries with different SOC were stored for the same duration, followed by capacity tests and internal resistance tests. For the 100% SOC group, cells were charged to the upper cutoff voltage of 4.20 V, and the relaxed open circuit voltage (OCV) was approximately 4.16 V before storage.

**Table 4.** Calendar aging experiment setup.

| Type | Storage SOC | Relaxed Storage Voltage * | Temperature | Sample |
|---|---|---|---|---|
| 1<br>2 | 100% | 4.16 V | | 2 |
| 3<br>4 | 75% | 3.96 V | | 2 |
| 5<br>6 | 50% | 3.75 V | 25 °C or 55 °C | 2 |
| 7<br>8 | 25% | 3.50 V | | 2 |
| 9<br>10 | 0% | 2.97 V | | 2 |

* The relaxed storage voltage of 100% storage SOC is at 4.16 V, which is the relaxed OCV after charging to the upper cutoff voltage of 4.20 V and subsequent relaxation.

(3) High-temperature cycling experiment under various charge/discharge rates

To investigate degradation under different aging paths during high-temperature cycling, LIBs under different charge/discharge rates were tested; that is, 0.3C, 0.5C, 0.75C, 1C, 1.5C, and 3C, as shown in Table 5. When conducting the effect of charge rate on aging, the discharge current in each cycle was set to 3C. When conducting the effect of discharge rate, the charge current was set to 3C.

**Table 5.** Experimental setup of charge–discharge rate on battery aging.

| Type | Charge Rate | Discharge Rate | Charge/Discharge Cutoff Voltage | Temperature | Cycles | Samples |
|---|---|---|---|---|---|---|
| 1 | 3C | 3C | 4.2 V–2.5 V | 55 °C | 150 | 1 |
| 2 | 0.3C | 3C | 4.2 V–2.5 V | 55 °C | 150 | 1 |
| 3 | 0.5C | 3C | 4.2 V–2.5 V | 55 °C | 150 | 1 |
| 4 | 0.75C | 3C | 4.2 V–2.5 V | 55 °C | 150 | 1 |
| 5 | 1C | 3C | 4.2 V–2.5 V | 55 °C | 150 | 1 |
| 6 | 1.5C | 3C | 4.2 V–2.5 V | 55 °C | 150 | 1 |
| 7 | 3C | 0.3C | 4.2 V–2.5 V | 55 °C | 150 | 1 |
| 8 | 3C | 0.5C | 4.2 V–2.5 V | 55 °C | 150 | 1 |
| 9 | 3C | 0.75C | 4.2 V–2.5 V | 55 °C | 150 | 1 |
| 10 | 3C | 1C | 4.2 V–2.5 V | 55 °C | 150 | 1 |
| 11 | 3C | 1.5C | 4.2 V–2.5 V | 55 °C | 150 | 1 |

(4) Battery adiabatic thermal test

The heat–wait–search (H–W–S) test is an important adiabatic calorimetry method constructing adiabatic conditions and determining the key temperatures of exothermic reactions for LIBs. During the H–W–S test, the battery sample undergoes calibration from the initial reaction temperature, then enters the search phase for exothermic reactions and track phase for the thermal process. Precise temperature measurement of the battery self-heating behavior can help illustrate the adiabatic thermal stability and decomposition characteristics of LIBs.

(5) Battery basic electro-thermal parameter test

The incremental capacity (IC) curve of LIBs was obtained by taking the first derivative of the charge/discharge voltage-capacity curve, and the charge/discharge current was set to 0.04C (0.12 A), as shown in Table 6. Interpolation at 9 mV intervals was applied to the obtained IC curve.

**Table 6.** IC capacity increment test.

| Steps | Content |
|---|---|
| 1 | Put battery in a constant temperature chamber at 25 °C. Discharge at 0.3C constant current to 2.5 V, then rest for 1 h. |
| 2 | Set the chamber temperature to 25 °C. Apply constant current charge at 0.04C (0.12 A) with a cutoff voltage of 4.2 V, then rest for 1 h. |
| 3 | Constant current discharge at 0.04C with a cutoff voltage of 2.5 V, then rest for 1 h. |
| 4 | Repeat the test with the temperature in Step 2 but changed to 10 °C, 35 °C, 45 °C, and 55 °C to conduct IC tests at different temperatures. |

The polarization internal resistance and ohmic internal resistance of the LIBs can be obtained through hybrid pulse power characterization (HPPC) tests. In this study, the entropy change and enthalpy change of LIBs during high-temperature, high-rate cycling aging were calculated based on the Gibbs free energy equation, which establishes the relationship between thermodynamics and electrochemistry. The open-circuit voltage of LIBs $\Delta E_{OCV}$ is related to Gibbs free energy $\Delta G$ as follows:

$$\Delta G = -nF\Delta E_{OCV} \tag{1}$$

According to thermodynamic principles, Gibbs free energy $\Delta G$ is related to entropy change $\Delta S$ and enthalpy change $\Delta H$ as follows:

$$\Delta G = \Delta H - T\Delta S \tag{2}$$

Hence, entropy change and enthalpy change can be calculated by the following equations:

$$\Delta S = -\frac{\partial \Delta G}{\partial T} = -nF\frac{\partial \Delta E_{OCV}(DOD, T)}{\partial T} \tag{3}$$

$$\Delta H(SOC) = -F\left(E_{OCV} - T\frac{\partial E_{OCV}(DOD, T)}{\partial T}\right) \tag{4}$$

where $n$ is the number of electrons involved in the electrode reaction, $F$ is the Faraday constant, $\Delta E_{OCV}$ is the electromotive force of the battery, and $\partial E_{OCV}(DOD,T)/\partial T$ is the entropy heat coefficient. The entropy heat coefficient can be obtained through HPPC tests.

## 3. Experiment Results and Analysis

### *3.1. Electrical Parameters of LIBs Under High-Temperature and High-Rate Cycling*

#### 3.1.1. Trends of Open-Circuit Voltage

The open-circuit voltages (OCV) were extracted from the voltage curves at 11 SOC points during the HPPC test. Figure 2a–d show the OCV curves of batteries at different aging cycles under 25 °C, 35 °C, 45 °C, and 55 °C. The fresh battery always exhibits the widest OCV range at all temperatures. With increasing aging, the OCV curves become monotonically flatter, which indicates that temperature significantly affects the OCV trends. Under the high temperature of 55 °C, the OCV range of all batteries remains between 2.89 V and 4.18 V. At 100% SOC, the OCV values of the fresh battery and the battery at 150 cycles are 4.18 V and 4.14 V, respectively, giving a difference of 0.04 V. At high temperature, the instantaneous polarization is reduced because electrolyte viscosity decreases and lithium-ion diffusivity increases. However, prolonged high-temperature exposure promotes SEI

thickening, SEI reconstruction, LAM, and interfacial charge–transfer impedance growth, which increase cumulative polarization. Hence, battery polarization and voltage relaxation are weakened at high temperature within "instantaneous/initial polarization" but increased at "aging-induced cumulative polarization". Furthermore, the OCV curves of batteries at different aging cycles have intersection, which locates at approximately 64.3% SOC at 55 °C, corresponding to a voltage of 3.88 V.

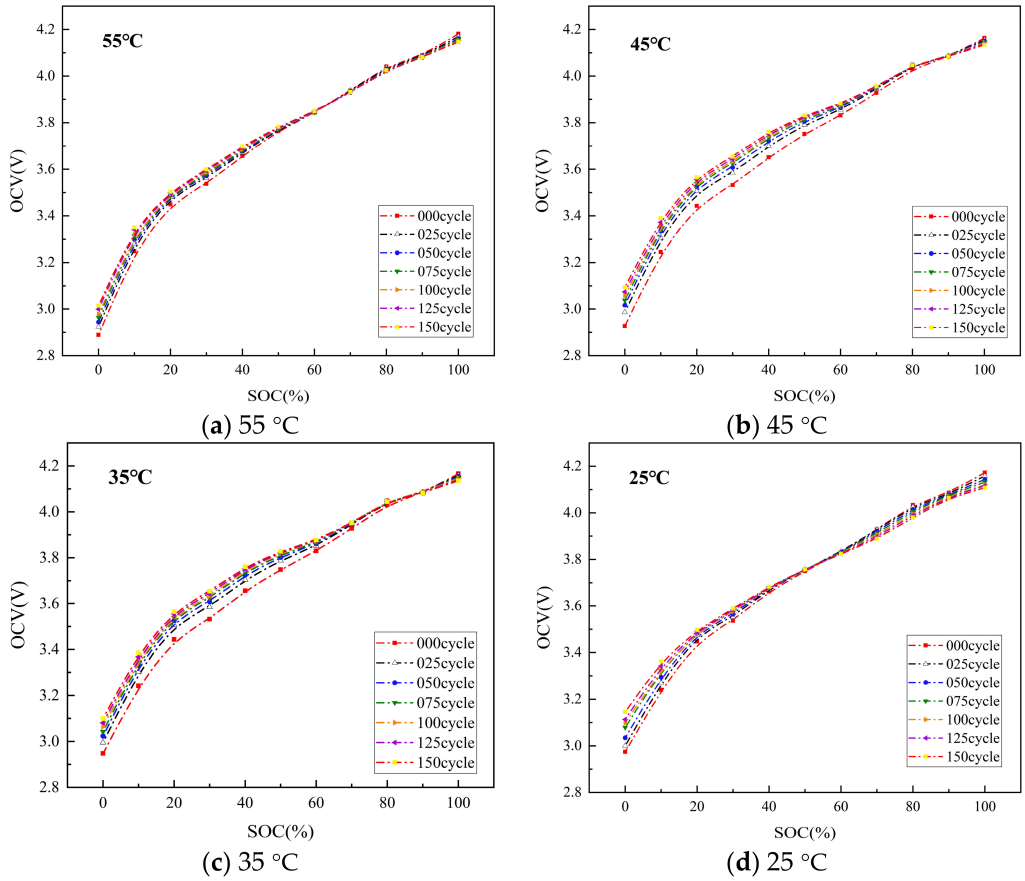



**Figure 2.** The open-circuit voltage curves of LIBs at different aging cycles under (**a**) 55 °C, (**b**) 45 °C, (**c**) 35 °C, and (**d**) 25 °C.

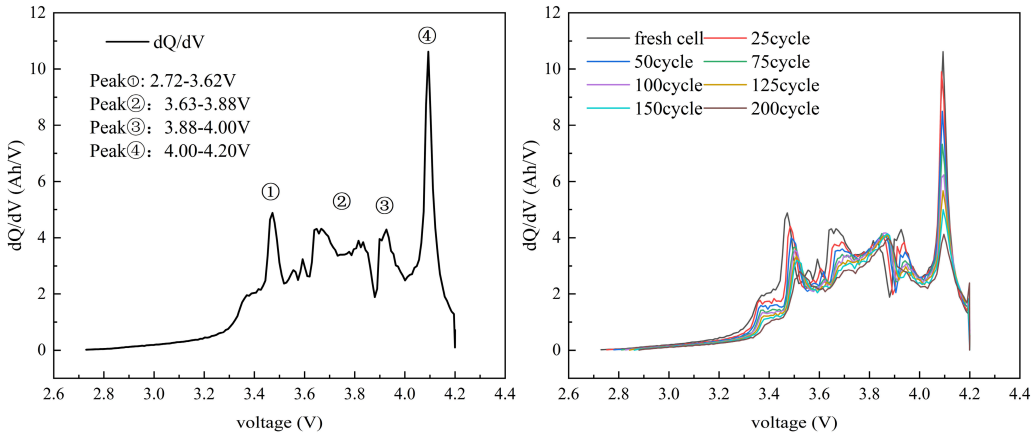
### 3.1.2. Trends of Incremental Capacity (IC) Curves

This section analyzes the IC curves for degradation characteristics of LIBs under high-temperature and high-rate cycling aging. IC curves of batteries with different aging cycles at 25 °C are presented, then IC curves of batteries cycled at different temperatures are compared.

1. IC curve at room temperature 25 °C

Figure 3a shows the typical positions of the four peaks, and Figure 3b shows the IC curves of eight battery groups with different aging degrees under 25 °C/0.04C charging conditions. With increasing aging of LIBs, the positions of Peaks ①, ②, and ③ shift rightwards, indicating increased resistance and polarization. The rightward shift of Peaks ① and ② are indicative of increased LLI and LAM. Regarding peak amplitudes, the left sides of Peak ② and Peak ③ decay severely with aging cycles, nearly disappearing at 150 and 200 cycles respectively, while the right side of Peak ② changes relatively little throughout aging. Peak ④ in the high-voltage region shows the largest amplitude decrease, maybe caused by LLI. In addition, a progressively higher small spike appears at 4.2 V in the charging IC curves of the cycling aging process. The position of Peak ③ corresponds to the voltage

range of 3.90 V–4.00 V, where the graphite electrode potential approaches 0 V. Peak ③ is associated with graphite staging and Ni/Co redox processes in the NCA cathode, whereas Peak ④ corresponds to the high-voltage phase transition of the Ni-rich layered cathode. The evolution of these peaks is indicative of combined LAM and LLI, but direct phase identification requires post mortem X-ray diffraction/X-ray photoelectron spectroscopy/transmission electron microscope (XRD/XPS/TEM) analysis.




(**a**) The position of the four peaks (**b**) IC curves at different aging cycles

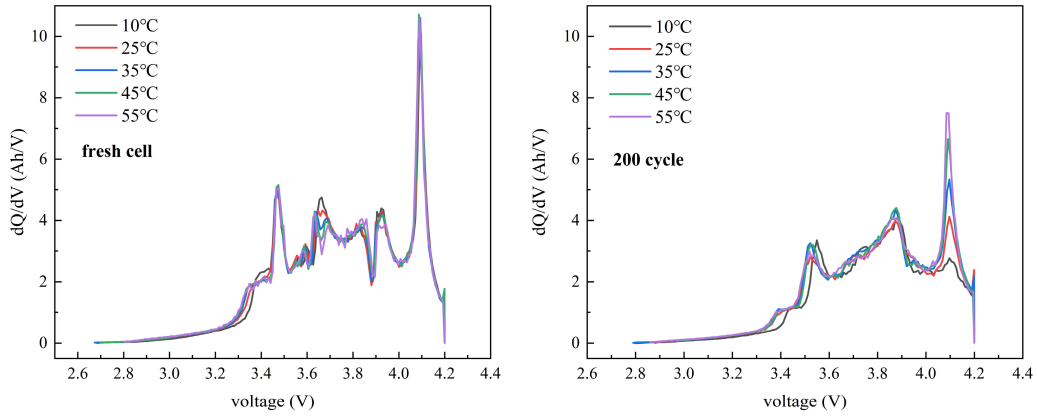
**Figure 3.** The IC curves of batteries at 25 °C, (**a**) the position of the four peaks, and (**b**) IC curves at different aging cycles.

2. Analysis of IC curves at different temperatures

Figure 4 shows a comparison of the IC curves of the fresh battery and the battery with 200 cycles at five temperatures 10 °C, 25 °C, 35 °C, 45 °C, and 55 °C. For the fresh battery, the peak shape and position are affected slightly by temperature. During charging at the five temperatures, the largest of the area differences of peaks ①–④ are only 0.087 Ah, which indicates that the fresh battery maintains good capacity retention at various temperatures under the low charging rate of 0.04C. For the battery with 200 aged cycles, SOH decreases to nearly 70%, and peak ④ shows obvious differences when charged at different temperatures. As the temperature decreases, the IC curves shift to the right, and peak ① shows an obvious rightward shift among the four peaks. The high temperature of 55 °C reduces the electrolyte viscosity, which decreases both the liquid-phase transfer impedance and the solid-phase diffusion impedance of the lithium ions. It indicates that high temperature and cycle aging affect battery polarization in opposite directions, and the net peak shift reflects the superposition of temperature-enhanced transport and aging-induced cumulative polarization.

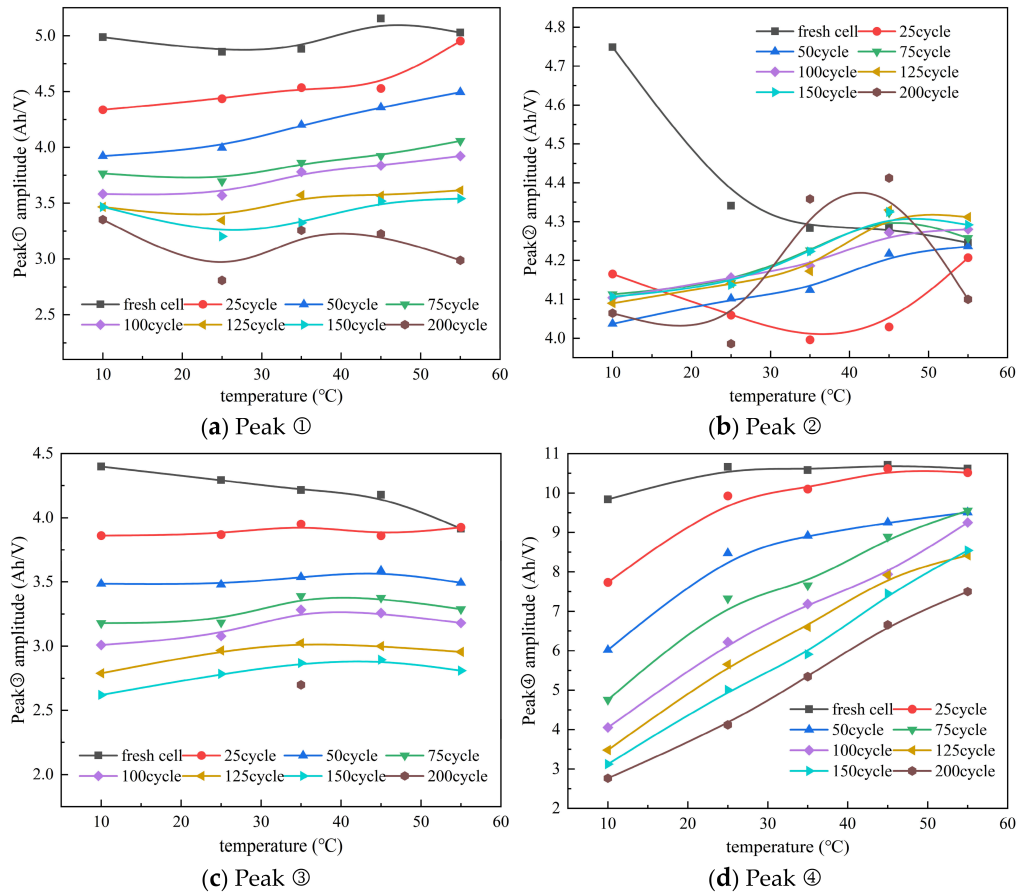
The amplitude variations of the IC curves at different temperatures for batteries at eight aging cycles are shown in Figure 5. More severe aging degrees lead to lower peak amplitudes of peaks ①, ③, and ④, indicating that high-temperature aging reduces the capacity increment per unit voltage. For peak ①, the peak amplitude fluctuates slightly across temperatures before 125 cycles, but after 200 cycles, the amplitude fluctuates considerably across temperatures, with an increase of 14.2 Ah/V from 10 °C to 55 °C. The evolution of peak ② keeps changing during aging and shows a non-monotonic trend. The reason is that, at high temperature (55 °C), parasitic reactions become dominant. Accelerated SEI growth and electrolyte decomposition consume active lithium, while interfacial degradation during cycling (200 cycle) increases polarization, collectively suppressing the capacity contribution of phase transitions and reducing IC peak intensity. Concurrently, phase transitions are confined to a narrower voltage window, concentrating the reaction and further lowering the peak height (dQ/dV). Except for the fresh battery, peak ③ of the other batteries remains

stable or increases slightly. Notably, the battery with 200 cycles shows a peak ③ with an amplitude of 2.70 Ah/V only at 35 °C, while the peak disappears at other temperatures, indicating that the phase transition corresponding to peak ③ has largely vanished. Peak ④ becomes increasingly dependent on temperature as aging progresses. The fresh battery shows a 7.9% increase from 10 °C to 55 °C, while the battery aged for 200 cycles shows a 271% increase. This indicates that increasing the temperature can moderately enhance the capacity increment in the high-voltage region for aged batteries.




(**a**) Fresh cell (**b**) batteries with 200 cycles

**Figure 4.** The comparison of IC curves of new batteries and batteries with aging cycles at different temperatures. (**a**) Fresh cell, and (**b**) batteries with 200 cycles.




(**a**) Peak ① (**b**) Peak ②

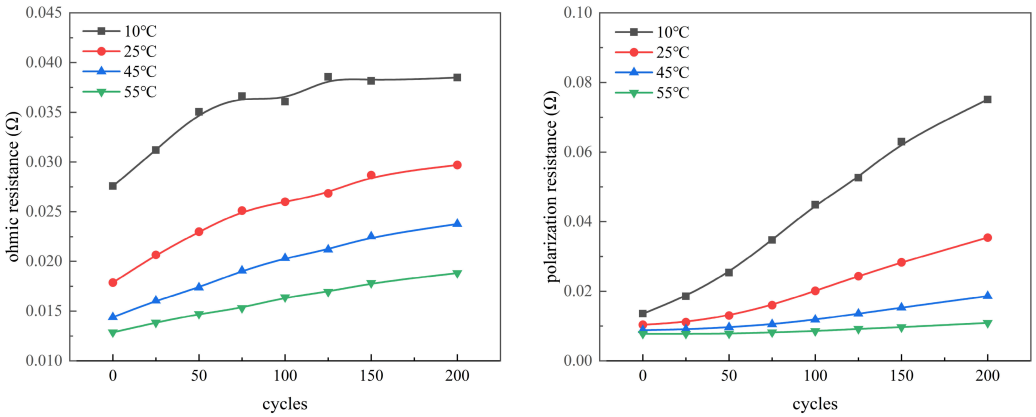
(**c**) Peak ③ (**d**) Peak ④

**Figure 5.** The amplitudes of the four peaks at different temperatures, (**a**) Peak ①; (**b**) Peak ②; (**c**) Peak ③; (**d**) Peak ④.

3.1.3. Trends of Internal Resistance

1. Internal resistance variation of aged batteries at different temperatures

Figure 6 presents the average ohmic resistance and average polarization resistance at 20–80% SOC for batteries at eight aging levels, measured at 0 °C, 10 °C, 25 °C, 40 °C, and 55 °C by HPPC tests. As the temperature increases, the ionic transport accelerates, and the average ohmic resistance decreases overall, while a slight increase appears at higher aging levels. At 55 °C, the maximum difference in average ohmic resistance is 6 mΩ. As shown in Figure 6b, with increasing aging level, lower temperatures (10 °C or 25 °C) have a greater effect on the average polarization resistance. In contrast, the curve at 55 °C remains nearly flat, indicating that aging has little influence on polarization resistance at high temperature.



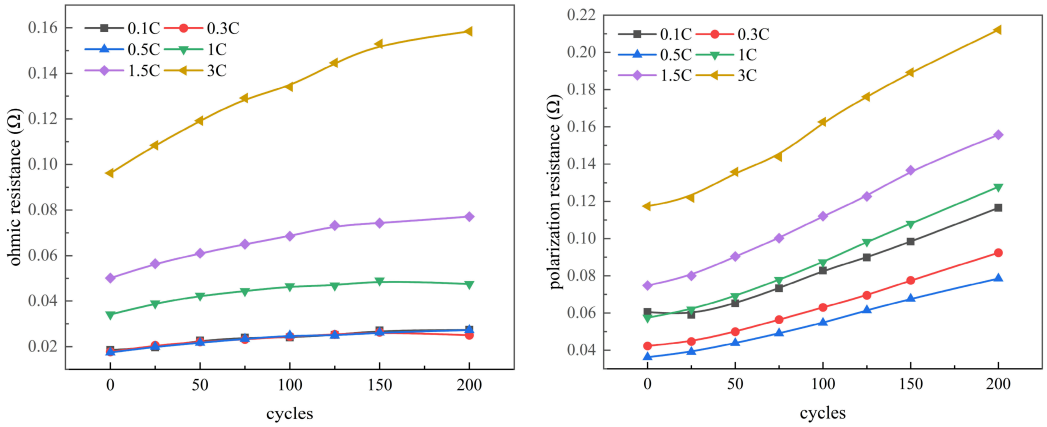

(**a**) Ohmic resistance (**b**) Polarization resistance

**Figure 6.** Internal resistance of aged batteries at different temperatures, (**a**) ohmic resistance, and (**b**) polarization resistance.

2. Internal resistance variation of aged batteries at different rates

Figure 7 shows the average ohmic resistance and polarization resistance at 20–80% SOC for batteries with eight aging cycles at rates of 0.1C, 0.3C, 0.5C, 1C, 1.5C, and 3C. For ohmic resistance, Figure 7a shows that the differences among batteries at eight aging cycles are very small, below 1.5C. The ohmic resistance at 1C is 40 mΩ, and it stays between 50 mΩ and 70 mΩ at 1.5C. Above 1.5C, the battery with 200 cycles shows an average ohmic resistance of 27 mΩ, and the difference reaches 62 mΩ at 3C. This may result from thermal expansion of the electrode surface caused by the temperature rise under the high rates, which reduces the contact area and thus increases the ohmic resistance.

With more severe aging, the polarization resistance shows an increasing trend. At 0.5C, the polarization resistance of all batteries is the lowest, and the polarization resistance decreases from 0.1C to 0.5C. This is because concentration polarization and electrochemical polarization inside the battery reach a balance at 0.5C. At higher rates, current collection and distribution become more difficult, leading to increased current density in certain electrode regions and localized polarization, which increases the overall polarization resistance. In addition, excessively fast ion transport reduces the lithium-ion concentration near the electrodes, causing concentration polarization. At 0.5C, the polarization resistances of the battery with 200 cycles and the fresh battery are 78.5 mΩ and 36.3 mΩ, respectively. At 3C, the polarization resistances are 212.1 mΩ and 117.4 mΩ, respectively. The value at 3C is nearly double.



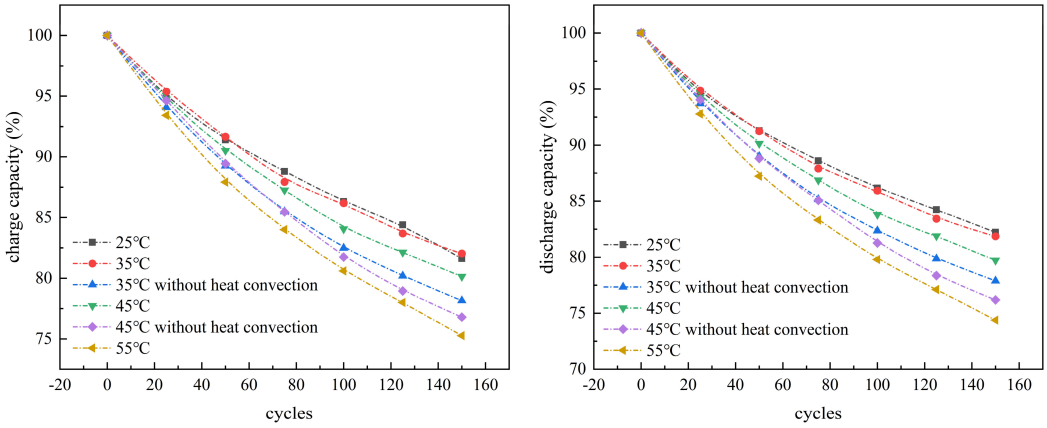

(**a**) Ohmic resistance (**b**) Polarization resistance

**Figure 7.** Internal resistance of aged batteries at different rates, (**a**) ohmic resistance, and (**b**) polarization resistance.

### *3.2. Effect of High Temperature on the Cycle Aging Characteristics of LIBs*

#### 3.2.1. Capacity Degradation of LIBs with Cycling at Different Temperatures

The reference capacity is the charge and discharge capacity in the first aging cycle. Figure 8 shows the relative capacity degradation (SOH) after 150 aging cycles at different temperatures. The cells aged at 25 °C and 35 °C with heat convection exhibit nearly the same capacity degradation rate in the first 50 cycles, which indicates that the temperature rise caused by heat generation and degradation rates differs little between 25 °C and 35 °C. The capacity variation of cells with heat convection and without heat convection at 25 °C, 35 °C, 45 °C and 55 °C are listed in Table 7 for comparison. The cells without heat convection show similar degradation rates in the first 75 cycles, both decaying to 85% of the initial capacity. In contrast, the cells with heat convection decay less than those without heat convection in the 75 cycles. Concerning the temperature shown in Table 7, heat accumulation in LIBs accelerates the loss of active material and speeds up capacity degradation. The cell aged at 55 °C with heat convection retains only 74.39% capacity after 150 aging cycles.



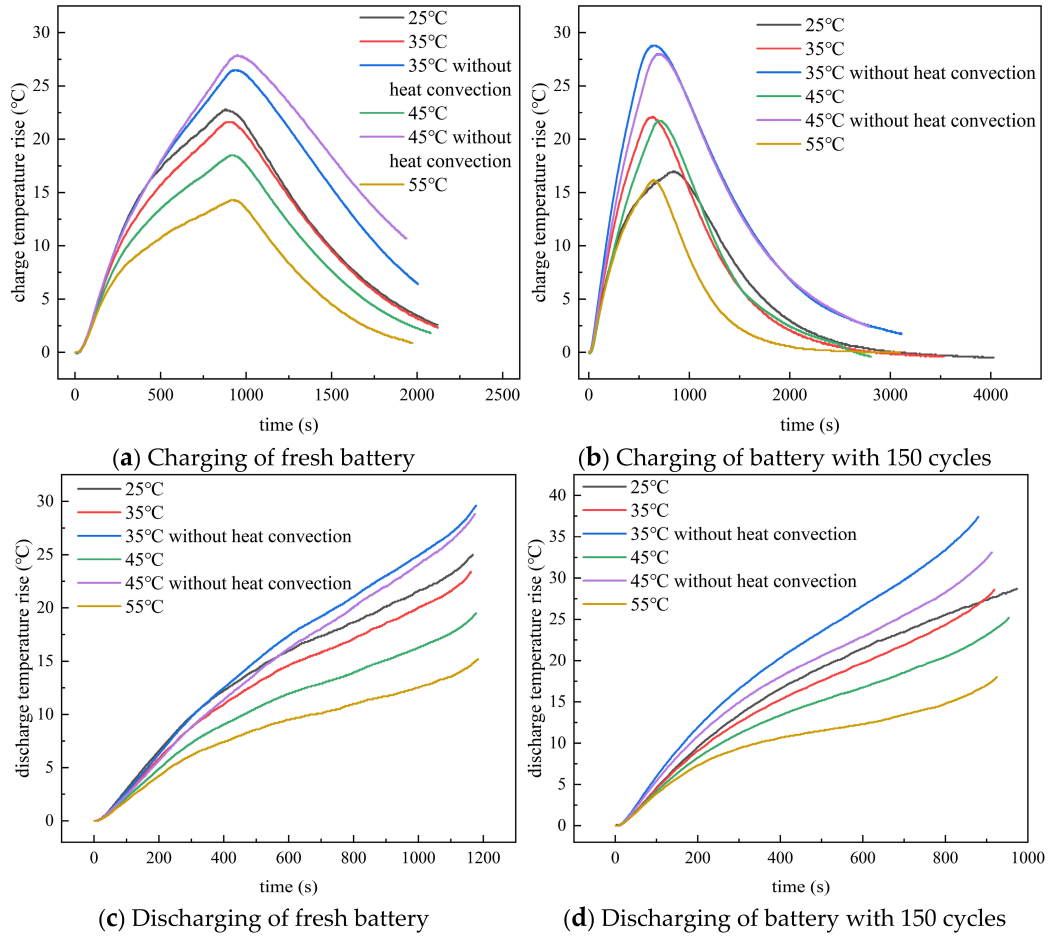

(**a**) Charging (**b**) Discharging

**Figure 8.** Capacity trends of LIBs aged at different temperatures, (**a**) charging, and (**b**) discharging.

**Table 7.** Capacity variation of LIBs under high-temperature cycling.

| Temperature | 25 °C | 35 °C | 35 °C (Without Heat Convection) | 45 °C | 45 °C (Without Heat Convection) | 55 °C |
|---|---|---|---|---|---|---|
| 75 cycles | 88.79% | 87.90% | 85.00% | 86.90% | 85% | 84.00% |
| 150 cycles | 81.61% | 82.03% | 78.16% | 80.14% | 76.80% | 74.39% |
| Temperature rise | 25 °C | 23.3 °C | 29.6 °C | 19.5 °C | 28.8 °C | 15.1 °C |

Figure 9 illustrates the temperature rises of LIBs under different temperatures, comparing the fresh state and the 150th cycle. Under heat convection, higher temperature leads to lower temperature rise. As shown in Table 7, the temperature rise decreases with higher temperature because high temperature enhances electrolyte fluidity and reduces the concentration polarization resistance. For example, the internal resistance of a fresh cell decreases from 0.028 Ω at 25 °C to 0.019 Ω at 55 °C. Moreover, the temperature rise without heat convection exceeds that with heat convection by more than 5 °C. During the 150th cycle test, the maximum discharge temperature rise reaches 37.4 °C, confirming the critical role of heat convection in battery thermal management.




(**a**) Charging of fresh battery (**b**) Charging of battery with 150 cycles

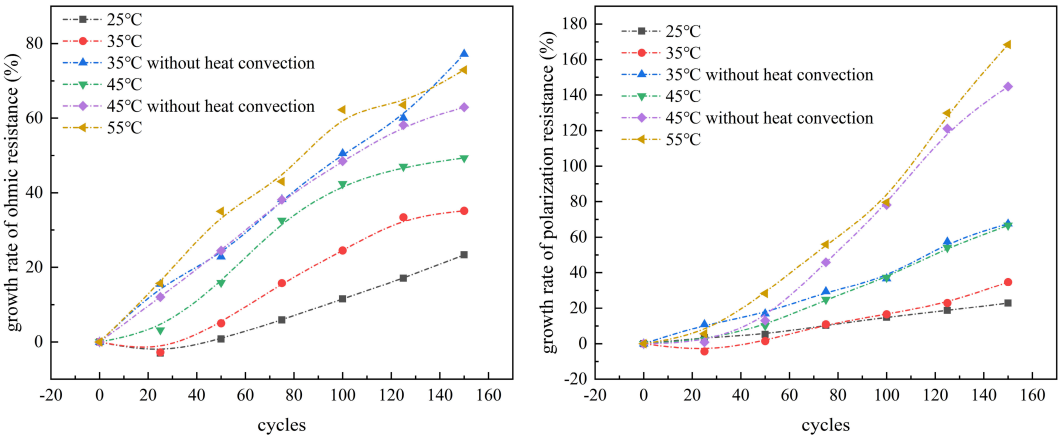
(**c**) Discharging of fresh battery (**d**) Discharging of battery with 150 cycles

**Figure 9.** Temperature rise between fresh battery and 150 cycles at different temperatures, (**a**) charging of fresh battery, (**b**) charging of battery with 150 cycles, (**c**) discharging of fresh battery, and (**d**) discharging of battery with 150 cycles.

### 3.2.2. Internal Resistance of LIB Cycling at Different Temperatures

Figure 10 shows the incremental trends of ohmic resistance and polarization resistance measured every 25 cycles. Cycling at varying temperatures induces distinct internal resis-

tance of LIBs due to differential side reactions. For ohmic resistance, the aging-induced growth rate at increasing temperatures exceeds that at room temperature of 25 °C. After 150 cycles, ohmic resistance at 55 °C increases by 72.93%, which is caused by LAM and SEI partial dissolution under high temperature. Then SEI would be regenerated at the peak discharge temperature of 78 °C, which reduces the electrode/electrolyte contact area and the ionic conductivity.




(**a**) Ohmic resistance (**b**) Polarization resistance

**Figure 10.** Internal resistance growth rate of LIBs aged at different temperatures, (**a**) ohmic resistance, and (**b**) polarization resistance.

The polarization resistance increases 22.9%, 34.7%, 66.6%, and 168.4% at 25 °C, 35 °C, 45 °C, and 55 °C at 150 cycles, respectively. Higher temperatures exacerbate LAM, electrode structural damage, charge-transfer inefficiency, and SEI inhomogeneity, thereby amplifying interfacial contact resistance and concentration polarization. Accordingly, higher temperatures during high-rate operation accelerate internal resistance growth in LIBs, with the growth rate rising progressively with temperature.

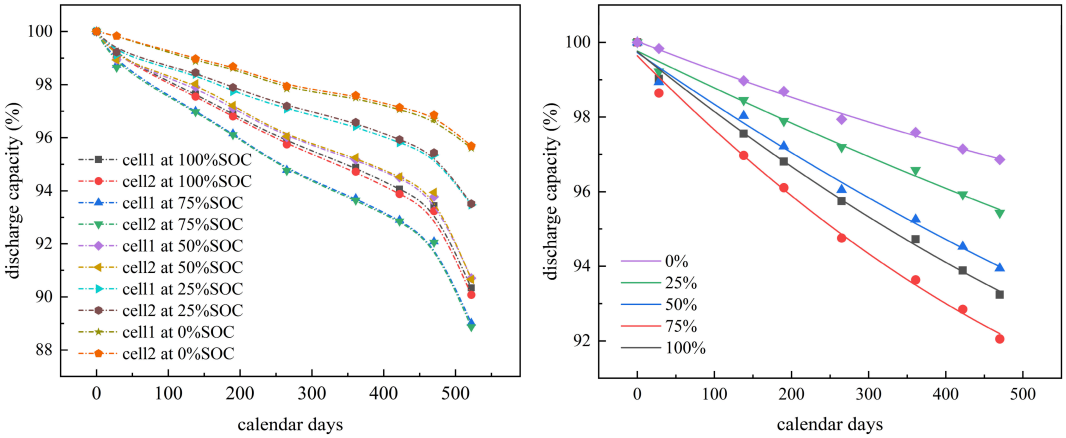
### *3.3. Effect of High Temperature on Calendar Aging of LIBs*

Temperature and storage SOC are key factors affecting the calendar aging rate of LIBs. Ten LIBs were divided into five groups and preconditioned to 100% SOC, 75% SOC, 50% SOC, 25% SOC, and 0% SOC. Calendar aging tests were conducted at temperature 25 °C and 55 °C. Capacity and HPPC tests were performed at specified aging intervals.

#### 3.3.1. Capacity Variation of LIBs Under Calendar Aging at Different Temperatures

Figure 11a presents the capacity variation of ten LIBs under calendar aging at different SOC. The aging environment during the first 470 days was 25 °C, and the cells were placed in a 55 °C chamber until 520 days. The 55 °C data were obtained after 470 days at 25 °C and therefore reflect the response of pre-aged cells. The design of this experiment tried to avoid the inconsistency among different cells, thus only one cell was stored both at 25 °C and 55 °C, sequentially. Capacity and HPPC tests were conducted on days 30, 140, 190, 265, 360, 420, 470, and 520. The average residual capacity retention of the two cells at each SOC is summarized in Table 8. The fastest capacity fading occurs at 75% SOC, followed by 100% SOC, at which the capacity retentions are 92.07% and 93.34%, respectively. Hence, the capacity fading rate does not increase monotonically with SOC but exhibits a maximum value around 75% SOC. Additionally, from day 470 to day 520 under 55 °C aging, the capacity fading rate increases sharply. The fitting curves of the first 470 days of aging data are shown in Figure 11b, and the monthly calendar aging fading rates are listed in Table 8.

The results indicate that the calendar aging rate at 25 °C is approximately linear over time across all SOC, with the 75% SOC cells still exhibiting the highest monthly fading rate.




(**a**) Capacity variation (**b**) Fitting curve

**Figure 11.** Capacity variation and fitting curve during calendar aging of LIBs with different SOC, (**a**) capacity variation, and (**b**) fitting curve.

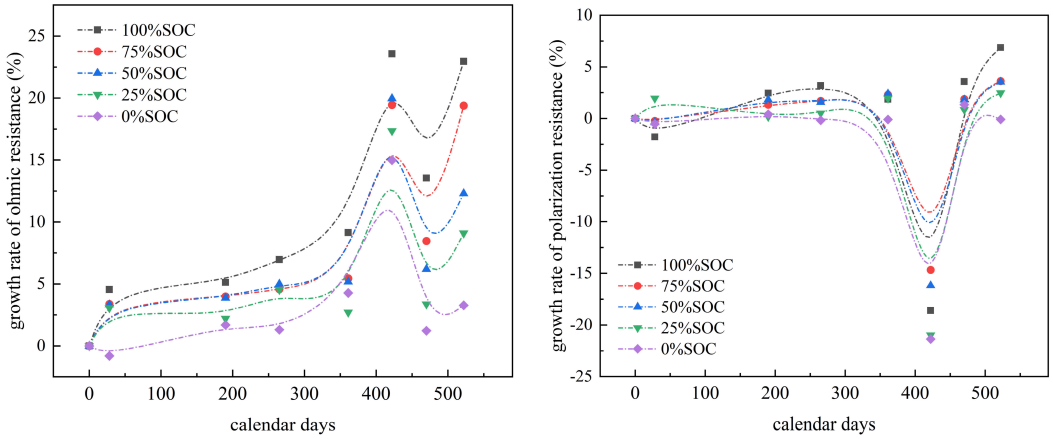
**Table 8.** Capacity variation of LIBs under calendar aging at 25 °C and 55 °C.

| SOC | 0% | 25% | 50% | 75% | 100% |
|---|---|---|---|---|---|
| capacity retention at 25 °C | 96.78% | 95.39% | 93.86% | 92.07% | 93.34% |
| capacity loss at 55 °C | 1.17% | 1.92% | 3.28% | 3.18% | 3.20% |
| aging rate per month | 0.2016% | 0.2715% | 0.3666% | 0.4767% | 0.4107% |

The degradation induced by high temperature is caused by accelerated side reactions, rapid LAM, and increased electronic conductivity of the SEI, which promotes higher electrolyte decomposition at the SEI/electrolyte interface. The accelerated calendar aging at approximately 75% SOC arises from high cell potential, which facilitates electrolyte reduction and SEI growth, thereby expediting LAM. Consequently, high temperature and high SOC (i.e., high storage voltage) readily trigger rapid degradation of LIBs. Battery storage should therefore be maintained at ambient temperature and avoid high SOC regions, particularly around 75%.

### 3.3.2. Internal Resistance of LIBs Under Calendar Aging at Different Temperatures

This section analyzes cell internal resistance at different SOC. Figure 12 and Table 9 show ohmic and polarization resistance growth for five LIBs at 100%, 75%, 50%, 25%, and 0% SOC. Higher SOC causes faster resistance growth. After 470 days at 25 °C and 50 days at 55 °C, high-SOC cells show larger ohmic resistance increases, while the 0% SOC cell shows the slowest growth, indicating that elevated SOC amplifies high-temperature resistance growth. After about one year of storage, ohmic resistance decreases rapidly while polarization resistance increases. After 50 days at high temperature, ohmic resistance rises markedly but polarization resistance rises only slightly, mainly due to SEI thickening at the negative electrode, which increases interfacial ionic resistance. Polarization resistance changes little during calendar aging.




(**a**) Ohmic resistance (**b**) Polarization resistance

**Figure 12.** Internal resistance growth rate of LIBs under calendar aging, (**a**) ohmic resistance, and (**b**) polarization resistance.

**Table 9.** Ohmic resistance of LIBs under calendar aging at 25 °C and 55 °C.

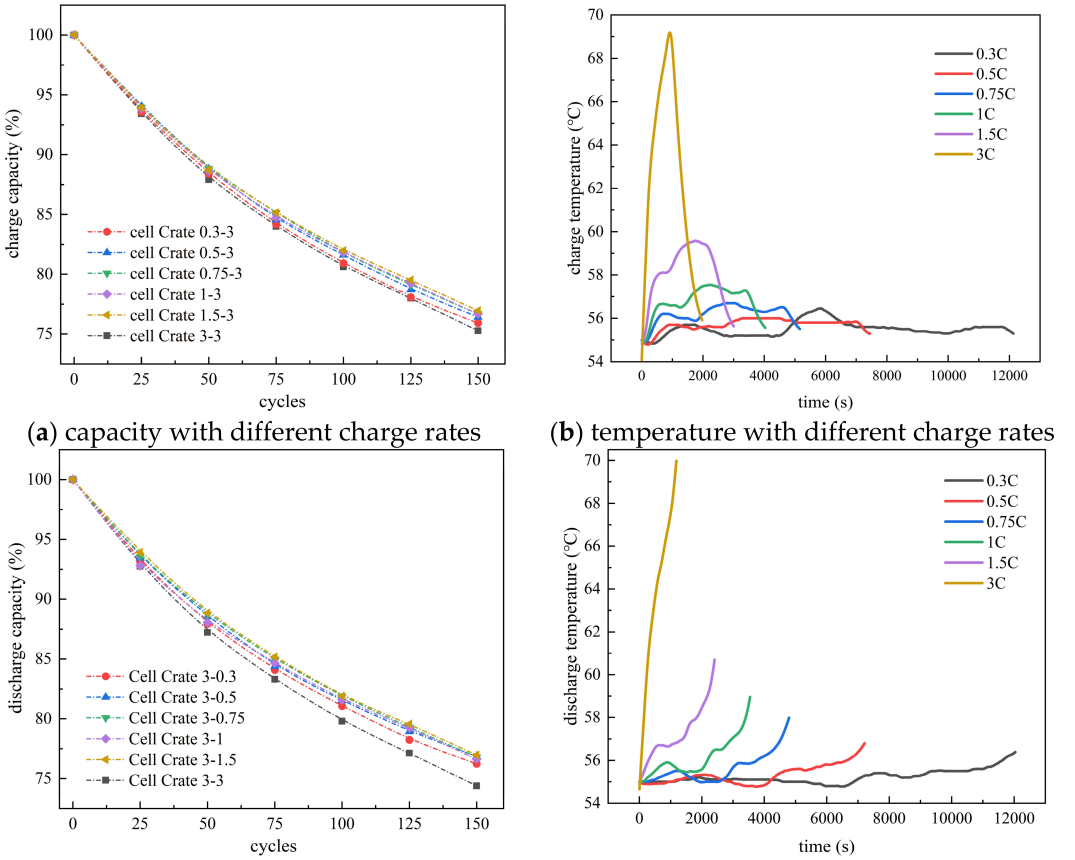
| SOC | 0% | 25% | 50% | 75% | 100% |
|---|---|---|---|---|---|
| Growth rate of ohmic at 25 °C | 1.26% | 2.41% | 4.52% | 5.96% | 9.75% |
| Growth rate of ohmic at 55 °C | 0.73% | 4.16% | 4.45% | 7.43% | 7.08% |

### *3.4. Effect of Charge/Discharge Rate on Cycling Characteristics of LIBs*

This section investigates the effect of charge/discharge rate on high-temperature cycling of LIBs. All cyclic aging tests were conducted at 55 °C. Five cells were cycled for 150 times at charge rates of 0.3C, 0.5C, 0.75C, 1C, and 1.5C, respectively, with a fixed discharge rate of 3C. Another five cells were cycled for 150 times at discharge rates of 0.3C, 0.5C, 0.75C, 1C, and 1.5C, respectively, with a fixed charge rate of 3C. An additional reference cell was cycled at 55 °C with a 3C–3C charge/discharge rate for 150 cycles. All 11 cells were subjected to capacity and HPPC internal resistance tests every 25 cycles under 2 °C/0.3C charge/discharge conditions. Capacity and internal resistance evolution data were recorded throughout the aging process.

#### 3.4.1. Capacity Variation of LIBs After Cycling at Different Rates

Figure 13 and Table 10 present the capacity variations and temperature rise during cycling at different charge rates under 55 °C. The fastest capacity fading occurs at the 3C charge rate, followed by 0.3C. For charge rates between 0.5C and 1.5C, the capacity fading rate decreases with increasing rate, with the slowest fading observed experimentally at 1.5C. Cells cycled at 0.5C–1.5C reach 80% SOH after approximately 100 cycles. The difference in capacity fading rate among all charge rates at 55 °C is within 1%. It should be noted that, based on current experiment results, the rate-dependent differences are less than 1% and require replicate testing for statistical confidence. The maximum charging temperature reaches 75 °C, which significantly accelerates SEI decomposition and reconstruction. According to Figure 13b, temperature variation substantially affects the aging rate. The temperature rises and duration for 0.3C–3C rates are summarized in Table 10. The 0.3C charge rate yields the longest exposure to elevated temperature, with charging duration approximately 1.6 times that of 0.5C, 3 times that of 1C, and 6.1 times that of 3C.




(**a**) capacity with different charge rates (**b**) temperature with different charge rates

(**c**) capacity with different discharge rates (**d**) temperature with different discharge rates

**Figure 13.** Capacity variation and temperature rise of LIBs under different charge/discharge rates at high temperature, (**a**) capacity with different charge rates, (**b**) temperature with different charge rates, (**c**) capacity with different discharge rates, and (**d**) temperature with different discharge rates.

**Table 10.** Capacity variation and temperature rise of LIBs under different charge rates.

| Charging Rate | 0.3C | 0.5C | 0.75C | 1C | 1.5C | 3C |
|---|---|---|---|---|---|---|
| Capacity at 150 cycles | 75.92% | 76.41% | 76.68% | 76.68% | 76.96% | 75.27% |
| Max temperature rise | 56.5 °C | 56.3 °C | 56.7 °C | 57.6 °C | 59.6 °C | 69.3 °C |
| Duration of temperature rise | 12,130 s | 7449 s | 5160 s | 4032 s | 3006 s | 1973 s |

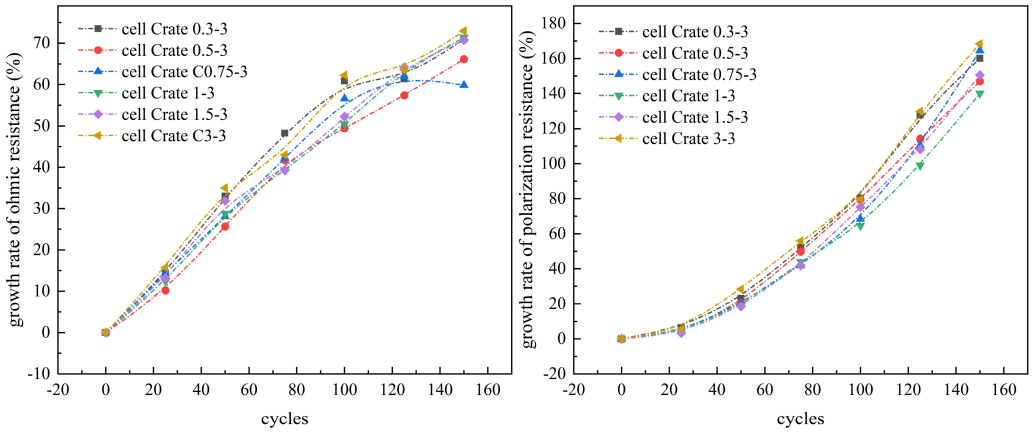
Figure 13c,d show the capacity variation and temperature during cycling at different discharge rates (55 °C). Capacity fading follows a trend similar to that under different charge rates. Based on the experimental results, aging rates from fastest to slowest are 3C, 0.3C, 1C, 0.5C, 0.75C, and 1.5C. Cells at 0.5C–1.5C discharge rates reach 80% SOH at 125 cycles, slower than their charge-rate counterparts, indicating lower mechanical stress from discharge-induced electrode expansion. As listed in Table 11, 0.3C discharge duration exceeds 12,000 s, 3.4 times that at 1C and 10.2 times that at 3C. The faster degradation at 0.3C versus 0.5C–1.5C results from prolonged duration, which enhances electrolyte evaporation and SEI thickening at 55 °C. The 3C rate causes rapid capacity loss due to excessive current and high polarization. Thus, for continuous high-temperature cycling, an appropriate rate increase shortens charge/discharge duration. A balance among rate, duration, and temperature plateau effectively reduces the cyclic aging rate of LIBs under high temperatures.

**Table 11.** Capacity variation and temperature rise of LIBs under different discharge rates.

| Discharging Rate | 0.3C | 0.5C | 0.75C | 1C | 1.5C | 3C |
|---|---|---|---|---|---|---|
| Capacity at 150 cycles | 76.24% | 76.88% | 76.81% | 76.62% | 76.98% | 74.39% |
| Max temperature rise | 55.2 °C | 55.3 °C | 55.6 °C | 56.1 °C | 57.2 °C | 63.6 °C |
| Duration of temperature rise | 12,040 s | 7211 s | 4793 s | 3546 s | 2408 s | 1184 s |

3.4.2. Internal Resistance of LIBs Under Cycling at Different Charge/Discharge Rates

Figure 14 and Table 12 present ohmic and polarization resistance increments every 25 cycles at 55 °C under charge rates of 0.3C–3C. Internal resistance increases monotonically with aging across all rates. For ohmic resistance, 150 cycle increments at 0.3C, 1C, 1.5C, and 3C differ marginally, with lower values at 0.5C and 0.75C, suggesting limited charge-rate effect on SEI thickening. Polarization resistance growth after 150 cycles is roughly double that of ohmic resistance. At 1C, ohmic resistance grows fast (second only to 3C), but polarization resistance grows slowest. At 0.75C, ohmic resistance growth is lowest, but polarization resistance grows relatively fast (second only to 3C). Overall resistance growth across 0.3C–3C shows minor variation, as it results from the trade-off between high-temperature exposure time and charging-induced temperature rise—low rates reduce the temperature rise but prolong the SEI thickening duration.




(**a**) Ohmic resistance (**b**) Polarization resistance

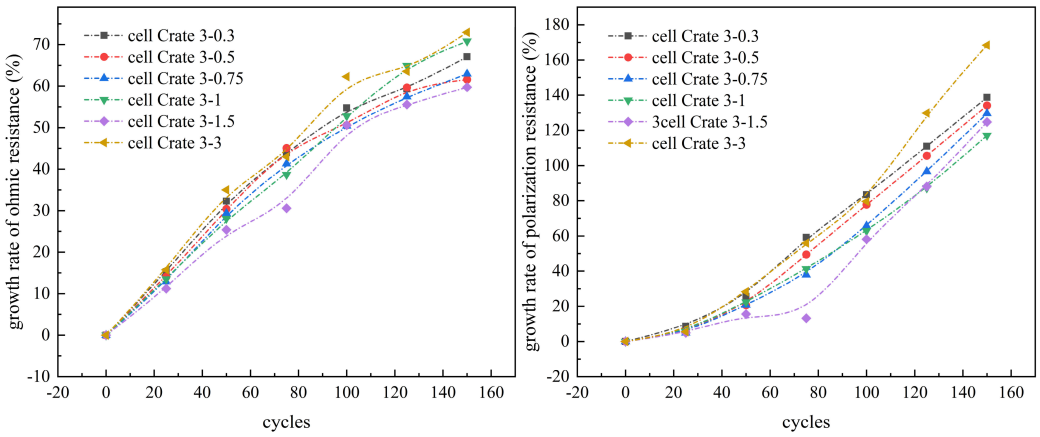
**Figure 14.** Internal resistance of LIBs at different charging rates under high temperature, (**a**) ohmic resistance, and (**b**) polarization resistance.

**Table 12.** Internal resistance of LIBs under different charge/discharge rates.

| Charge/Discharge Rates | | 0.3C | 0.5C | 0.75C | 1C | 1.5C | 3C |
|---|---|---|---|---|---|---|---|
| Charging with 150 cycles | Growth rate of ohmic resistance | 71.0% | 66.1% | 59.8% | 71.4% | 70.7% | 72.9% |
| | Growth rate of polarization | 160.1% | 147.0% | 164.5% | 140.0% | 150.5% | 168.4% |
| Discharging with 150 cycles | Growth rate of ohmic resistance | 67.1% | 61.6% | 62.9% | 70.8% | 59.7% | 72.9% |
| | Growth rate of polarization | 138.7% | 134.1% | 129.6% | 117.1% | 124.8% | 168.4% |

Figure 15 presents the ohmic and polarization resistance variations every 25 cycles for LIBs at 55 °C under different discharge rates (0.3C, 0.5C, 0.75C, 1C, 1.5C, and 3C) with a fixed charge rate of 3C. The fastest growth in both ohmic and polarization resistance occurs at 3C. At 0.3C, 0.5C, 0.75C, and 1.5C, the resistance growth rate decelerates after 100 cycles.

In contrast, the 1C rate shows no evident deceleration. The 1.5C rate exhibits the lowest growth rates for both ohmic and polarization resistance.




(**a**) Ohmic resistance (**b**) Polarization resistance

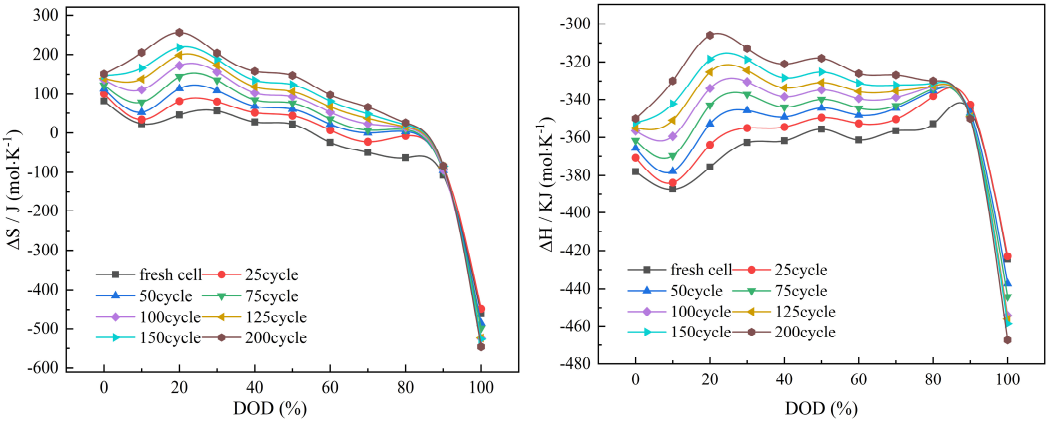
**Figure 15.** Internal resistance of LIBs at different discharging rates under high temperature, (**a**) ohmic resistance, and (**b**) polarization resistance.

### *3.5. Thermal Characteristics of LIBs Under High-Temperature, High-Rate Cycling*

#### 3.5.1. Heat Characteristics of LIBs Under High-Temperature, High-Rate Cycling

1. Entropy and Enthalpy Variation

Entropy and enthalpy changes during LIB charge/discharge indicate degradation of electrode materials, as shown in Figure 16. Based on Equations (3) and (4), the entropy and enthalpy variations of eight LIBs at different aging degrees as a function of depth of discharge (DOD) are shown in Figure 16.




(**a**) Entropy change (**b**) Enthalpy change

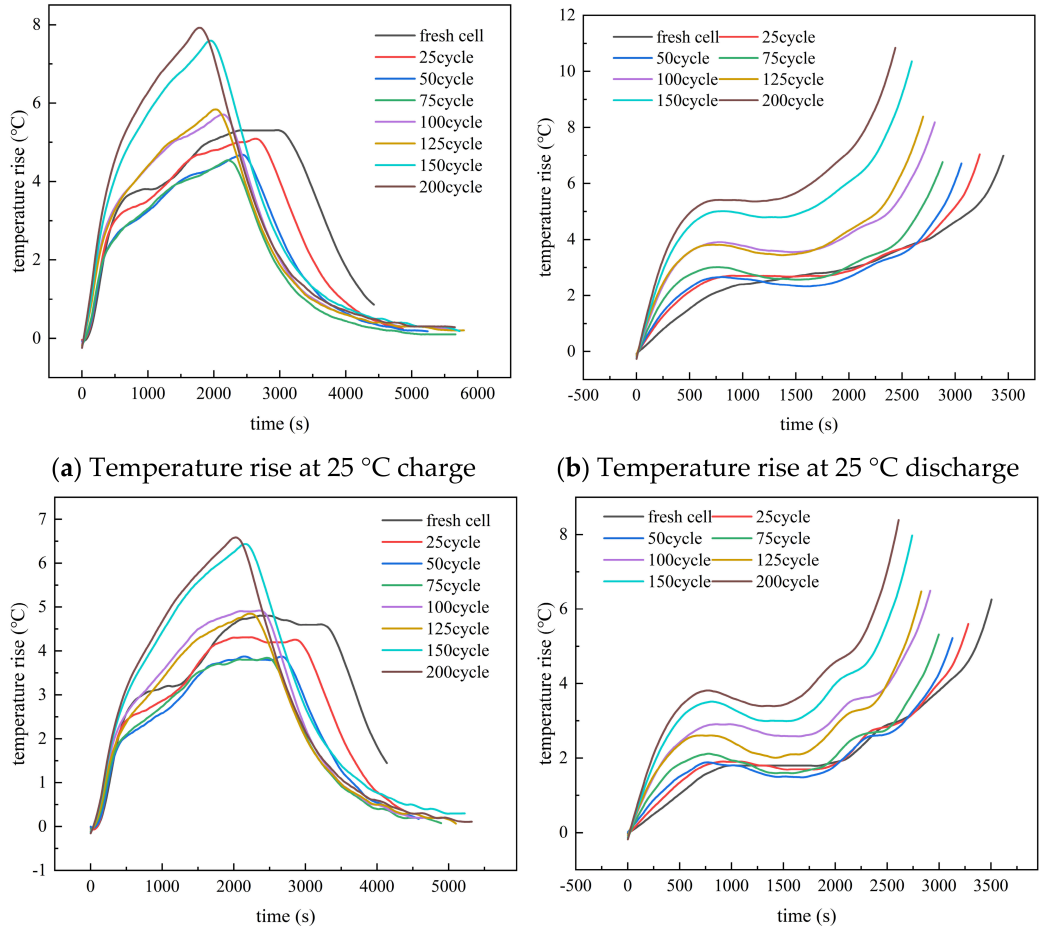
**Figure 16.** (**a**) Entropy change and (**b**) enthalpy change of LIBs with different cycles.

With increasing DOD, entropy changes from positive to negative at 50–60% DOD, indicating endothermic behavior below 50% DOD and exothermic behavior above 60% DOD. At 90–100% DOD, entropy drops sharply from −106.88 to −460.69 J/mol·K, matching the rapid temperature rise at the discharge end. With aging, the endothermic peak shifts from before 30% DOD to about 20% DOD, and the 90–100% DOD slope increases. At 100% DOD, entropy remains more negative, indicating intensified endothermic and exothermic intercalation under high-temperature cycling. Enthalpy follows a similar trend: at 90–100% DOD,

aging causes a sharp enthalpy drop and increased heat release, while enthalpy rises within 0–20% DOD.

2. Temperature rise during charge/discharge

Eight LIBs aged at 55 °C/3C were tested for temperature rise at various ambient temperatures. Tests used 1C, 4.2 V upper cut-off, 0.05C cut-off current, and 2.5 V lower cut-off. Figure 17 shows the charging temperature rise versus the aging degree. Cells aged within 100 cycles show small plateaus at higher ambient temperatures near 1000 s (~30% SOC), where the internal resistance decreases and the heat generation balances convection. During discharge, the temperature rise rate is non-monotonic. Greater aging raises high-SOC internal resistance and steepens initial temperature rise; higher ambient temperatures enhance electrochemical activity and reduce heat generation, lowering the temperature rise.



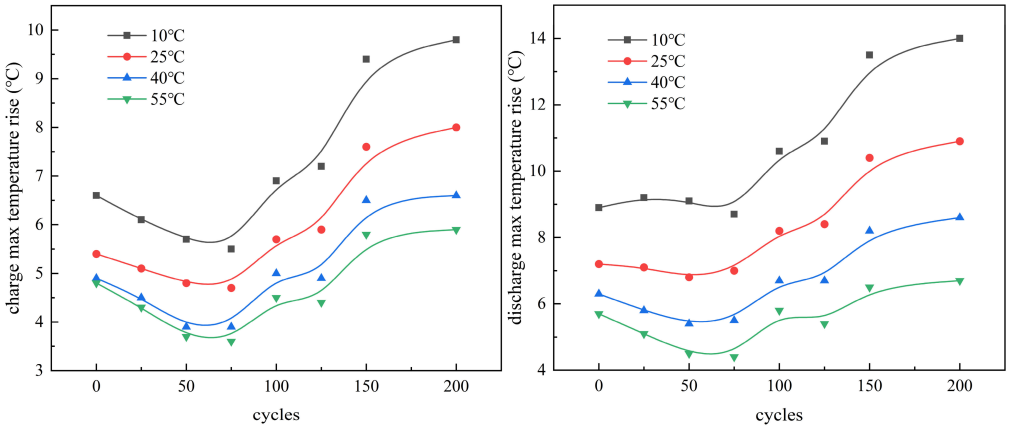

(**a**) Temperature rise at 25 °C charge (**b**) Temperature rise at 25 °C discharge

(**c**) Temperature rise at 55 °C charge (**d**) Temperature rise at 55 °C discharge

**Figure 17.** Charging temperature rise and maximum charging temperature rise at different ambient temperatures, (**a**) temperature rise at 25 °C charge, (**b**) temperature rise at 25 °C discharge, (**c**) temperature rise at 55 °C charge, and (**d**) temperature rise at 55 °C discharge.

Figure 18a shows the maximum temperature rise of aged cells versus cycle number at all ambient temperatures. The temperature rise has a turning point at ~75 cycles. Before 75 cycles, high temperature causes partial SEI dissolution and non-uniform redistribution. With further aging, a thicker and more stable SEI forms, aggravating the temperature rise. Cells at 150 and 200 cycles exhibit higher temperature rises at all temperatures than those below 125 cycles, indicating that the temperature rise increases notably when SOH drops

below 80%. Figure 18b shows the maximum discharge temperature rise versus cycle number. Fresh cells exhibit rises of 6.99 °C, 6.26 °C, and 5.75 °C at 25 °C, 35 °C, and 55 °C, while 200-cycle cells show 10.84 °C, 8.39 °C, and 6.72 °C, respectively, indicating that high-temperature cyclic aging significantly increases the temperature rise at lower ambient temperatures.




(**a**) Temperature rise during charge (**b**) Temperature rise during discharge

**Figure 18.** Maximum temperature rise during charge/discharge at different temperatures, (**a**) temperature rise during charge, and (**b**) temperature rise during discharge.

### 3.5.2. Thermal Stability of LIBs After High-Temperature High-Rate Cycling

Fresh battery, 50-cycle, 100-cycle, 150-cycle, and 200-cycle aged groups (SOH: 100%, 88.1%, 81.1%, 74.6%, and 70.6%) were selected for H–W–S adiabatic thermal stability tests at 0% SOC, aiming to evaluate the safety impact of high-temperature aging on fully discharged cells. At 0% SOC, lithium ions were fully intercalated into the positive electrode as $LiNi_{0.8}Co_{0.15}Al_{0.05}O_2$, with a stable voltage near 3.0 V after full rest.

Figure 19 and Table 13 show the adiabatic thermal decomposition curves and T1, T2, T3 evolution at five aging levels under 0% SOC. Since stored electrochemical energy is minimal at 0% SOC, the ARC response is interpreted as thermally induced self-heating and secondary decomposition rather than complete self-sustained thermal runaway. With aging, self-heating stability decreases, making self-heating more likely at the same temperature. T3 was determined from three thermocouples on the side, positive, and negative electrodes, with the side temperature taken as the maximum. High-temperature aging increases side-reaction products and flammable gases such as $H_2$ and CO, thus raising T3. Fresh cells, with fewer side products, show a lower T3.

**Table 13.** Thermal stability and decomposition parameters of LIBs with SOC = 0%.

| Cycles | T1 (°C) | T1 Time (s) | T2 (°C) | T2 Time (s) | T3 (°C) | T3 Time (s) |
|---|---|---|---|---|---|---|
| Fresh battery | 148.4 | 81,323 | 186.3 | 83,032 | 276.7 | 84,471 |
| 50 | 133.6 | 69,959 | 223.1 | 82,471 | 330.2 | 82,878 |
| 100 | 133.1 | 73,076 | 215.8 | 86,714 | 614.7 | 87,086 |
| 150 | 138.2 | 67,565 | 210.1 | 79,572 | 615.1 | 79,773 |
| 200 | 131.4 | 72,765 | 208.6 | 89,090 | 615.1 | 89,297 |

In summary, 0% SOC cells contain limited stored energy, and no severe flame ejection from the positive electrode is observed during adiabatic thermal decomposition. Heat release mainly results from active-material and electrolyte decomposition. The 0% SOC decomposition process shows a relatively long incubation period. The 150-cycle cell reaches T3 the fastest, possibly because the absence of significant venting avoids heat and gas release and thus prolongs heat re-accumulation. These results indicate that high-temperature

cycling reduces the thermal stability of fully discharged cells and enhances secondary decomposition and gas generation at 0% SOC.

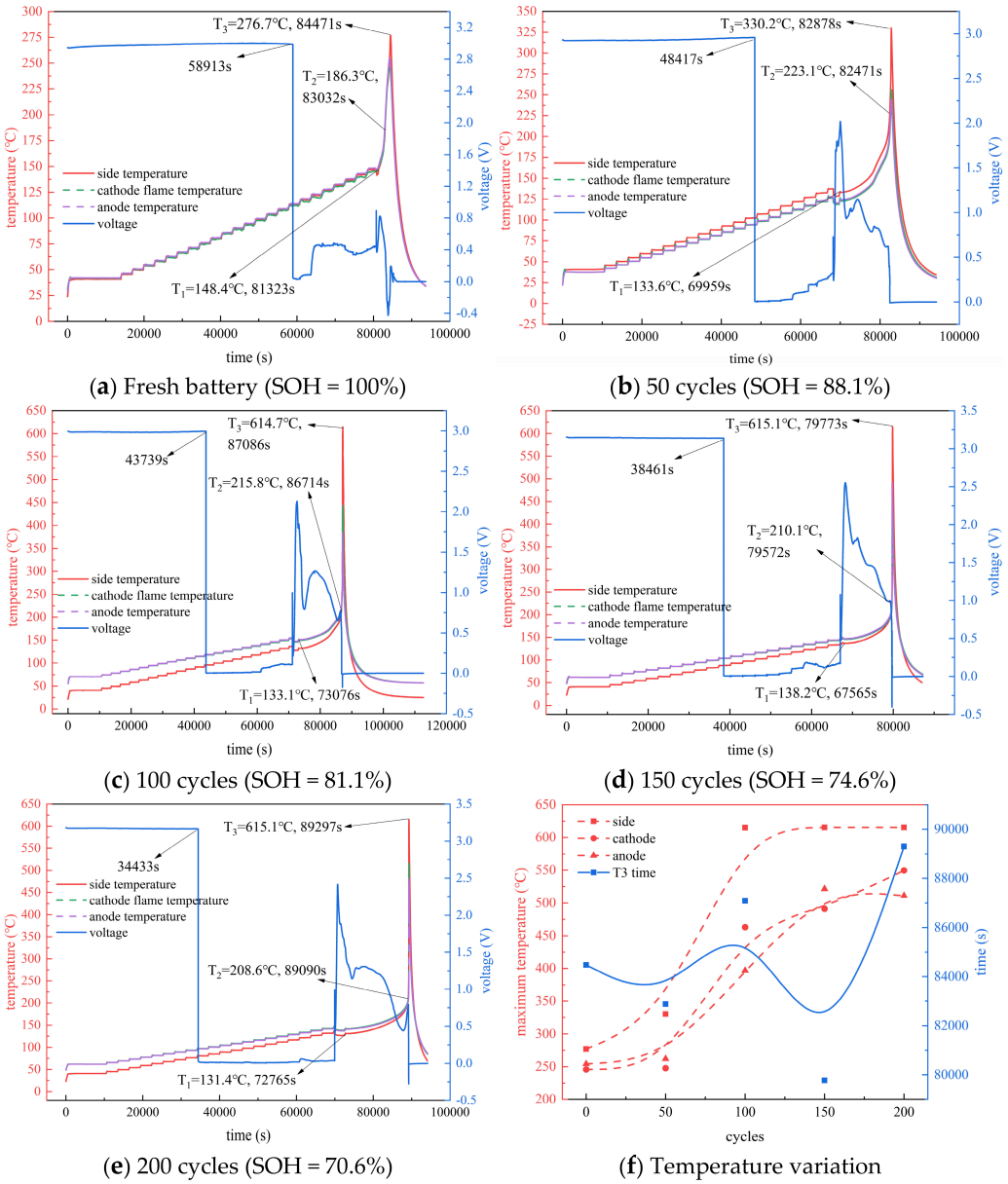



**Figure 19.** Adiabatic thermal curves of SOC = 0% of batteries with different cycles, (**a**) Fresh battery (SOH = 100%), (**b**) 50 cycles (SOH = 88.1%), (**c**) 100 cycles (SOH = 81.1%), (**d**) 150 cycles (SOH = 74.6%), (**e**) 200 cycles (SOH = 70.6%), and (**f**) Temperature variation.

### *3.6. Discussion*

(1) Capacity and internal resistance during high-temperature, high-rate cycling

LIB capacity fading accelerates under elevated ambient temperature and limited heat dissipation. High-temperature cycling raises the temperature plateau, accelerating capacity fade and resistance growth. Elevated temperature promotes passive film formation, exacerbating concentration polarization; polarization resistance grows more than ohmic resistance. Forced convection suppresses temperature rise, mitigating capacity fade and resistance growth. In cycling aging, repeated current excitation induces continuous SEI fracture/repair and interfacial charge-transfer degradation, which preferentially increases polarization resistance.

(2) Capacity and internal resistance during high-temperature calendar aging

High-temperature calendar aging accelerates capacity fade via SEI thickening and side reactions. Resistance growth increases, with ohmic resistance affected more than polarization resistance. High SOC lowers anode potential, promoting SEI growth and active lithium consumption, thus raising ohmic resistance. Capacity fade and resistance growth are non-monotonic, with SOC peaking near 75% SOC. In calendar aging, the absence of repeated current excitation shifts the dominant degradation toward SEI thickening, electrolyte decomposition/drying, and current-collector/interface corrosion, which preferentially increase ohmic resistance. The dominant resistance component is aging-regime dependent: cycling primarily amplifies polarization resistance, whereas calendar aging primarily amplifies ohmic resistance.

(3) Capacity and internal resistance under different rates at high-temperature cycling

Capacity fading and internal resistance growth under different charge/discharge rates at high temperature are generally fast and comparable. This is because both are cumulative over time—higher rates shorten duration, while lower rates prolong it, resulting in similar overall degradation. Additionally, capacity fading and resistance changes induced by discharge rate variation are smaller than those induced by charge rate variation.

(4) Thermal characteristics after high-temperature, high-rate cycling

High-temperature cyclic aging intensifies both endothermic intercalation and exothermic reactions, increasing the magnitude and rate of enthalpy and entropy changes. Maximum temperature rise increases monotonically with charge rate. For cells at 0% SOC undergoing thermal runaway (TR), pressure relief valve ejection precedes self-heating in all cases. With increasing aging, T1 and T2 decrease, indicating reduced material stability, while T3 increases, reflecting greater side reaction products and flammable gases. Voltage drop also occurs earlier, confirming that high-temperature cyclic aging elevates TR risk.

After all, all the measured quantities including capacity, resistance, IC curves, temperature, and ARC parameters were analyzed and based on the experimental results in this work. Proposed mechanisms such as SEI reconstruction, electrolyte drying, and electrode expansion are hypotheses supported by experimental results but cannot be directly deduced from this work. Further characterization methods such as XRD, XPS, Scanning Electron Microscope (SEM), Inductively Coupled Plasma (ICP), or differential voltage analysis, are required for quantitative separation of LLI and LAM, or mechanism investigation.

## 4. Conclusions

For the degradation evolution, calendar lifetime, and safety characteristics of LIBs at high temperature, this paper provides experimental results and analysis of the 18650 cell under various working conditions. High temperature (55 °C) with temperature rate, cycle number, and charging/discharging rate were taken into consideration to demonstrate cycling aging, calendar lifetime, and thermal characteristics. Capacity loss, internal resistance growth (including ohmic and polarization resistance), and incremental capacity analysis (ICA) were selected as the cycling degradation and calendar life index of LIBs. The aging laws both under cycling and calendar are provided for LIB usage and storage under high temperature. Thermal characteristics were analyzed by entropy change, enthalpy change, and temperature rate during high-temperature cycling. Moreover, adiabatic thermal experimental results under 0% SOC were also conducted for further safety analysis. Finally, four main contributions of this work were discussed as (i) unified experimental matrix; (ii) non-monotonic calendar aging near 75% SOC; (iii) rate-dependent trade-off; (iv) storage/operation recommendations. Several recommendations were concluded as reference for further research on cycling management and calendar storage strategies of BMS.

**Author Contributions:** Conceptualization, methodology, validation, formal analysis, investigation, R.W. and B.X.; resources, data curation, B.X.; writing—original draft preparation, R.W.; writing—review and editing, supervision, B.X. All authors have read and agreed to the published version of the manuscript.

**Funding:** This research received no external funding.

**Data Availability Statement:** The original contributions presented in this study are included in the article. Further inquiries can be directed to the corresponding author.

**Conflicts of Interest:** The authors declare no conflicts of interest.

## References

1. Alawi, A.; Saeed, A.; Sharqawy, M.H.; Al Janaideh, M. A comprehensive review of thermal management challenges and safety considerations in lithium-ion batteries for electric vehicles. *Batteries* **2025**, *11*, 275. [CrossRef]
2. Zhang, G.; Wei, X.; Wang, X.; Chen, S.; Zhu, J.; Dai, H. Evolution mechanism and non-destructive assessment of thermal safety for lithium-ion batteries during the whole lifecycle. *Nano Energy* **2024**, *126*, 109621. [CrossRef]
3. Qian, G.; Zheng, Y.; Li, X.; Sun, Y.; Han, X.; Ouyang, M. State of health estimation for lithium-ion batteries using impedance-based simplified timescale information. *Appl. Energy* **2025**, *382*, 125272. [CrossRef]
4. Liu, S.; Nie, Y.; Tang, A.; Li, J.; Yu, Q.; Wang, C. Online health prognosis for lithium-ion batteries under dynamic discharge conditions over wide temperature range. *eTransportation* **2023**, *18*, 100296. [CrossRef]
5. Qu, Y.; Xing, B.; Xia, Y.; Zhou, Q. How does room temperature cycling ageing affect lithium-ion battery behaviors under extreme indentation? *eTransportation* **2024**, *20*, 100331. [CrossRef]
6. Guo, J.; Ping, P.; Ren, J.; Ren, X.; Gao, W.; Kong, D.; Wang, D.; Feng, Z. High-temperature calendar aging at low state-of-charge: Electrochemical degradation, thermal safety implications, and optimal SOC ranges for lithium-ion battery storage and transport. *J. Energy Storage* **2025**, *125*, 116988. [CrossRef]
7. Ma, W.; Yang, X.; Tao, X.; Xie, S. The effect of low-temperature starting on the thermal safety of lithium-ion batteries. *Energy* **2024**, *311*, 133427. [CrossRef]
8. Ji, C.; Liu, D.; Liu, Y.; Wang, S.; Wang, Y.; Zhang, Z.; Wang, B. Effect of low temperature and high-rate cyclic aging on thermal characteristics and safety of lithium-ion batteries. *Process Saf. Environ. Prot.* **2024**, *188*, 1514–1526. [CrossRef]
9. Liu, J.; Zhou, L.; Zhang, Y.; Wang, J.; Wang, Z. Aging behavior and mechanisms of lithium-ion battery under multi-aging path. *J. Clean. Prod.* **2023**, *423*, 138678. [CrossRef]
10. Kim, S.; Jung, H.; Lee, M.; Choi, Y.Y.; Choi, J.I. Model-free reconstruction of capacity degradation trajectory of lithium-ion batteries using early cycle data. *eTransportation* **2023**, *17*, 100243. [CrossRef]
11. Wang, Z.; Zhao, Q.; Wang, S.; Song, Y.; Shi, B.; He, J. Aging and post-aging thermal safety of lithium-ion batteries under complex operating conditions: A comprehensive review. *J. Power Sources* **2024**, *623*, 235453. [CrossRef]
12. Carter, R.; Kingston, T.A.; Atkinson, R.W.; Parmananda, M.; Dubarry, M.; Fear, C.; Mukherjee, P.P.; Love, C.T. Directionality of thermal gradients in lithium-ion batteries dictates diverging degradation modes. *Cell Rep. Phys. Sci.* **2021**, *2*, 100351. [CrossRef]
13. Zhang, Z.; Ji, C.; Liu, Y.; Wang, Y.; Wang, B.; Liu, D. Effect of aging path on degradation characteristics of lithium-ion batteries in low-temperature environments. *Batteries* **2024**, *10*, 107. [CrossRef]
14. Bae, Y.S.; Lee, S.; Moon, J. Developing an Innovative Seq2Seq Model to Predict the Remaining Useful Life of Low-Charged Battery Performance Using High-Speed Degradation Data. *Batteries* **2024**, *10*, 389. [CrossRef]
15. Fly, A.; Wimarshana, B.; Bin-Mat-Arishad, I.; Broad, R.J. Influence of periodic temperature variations on calendar ageing of lithium-ion batteries. *J. Power Sources* **2025**, *657*, 238147. [CrossRef]
16. Zhang, G.; Wei, X.; Chen, S.; Wei, G.; Zhu, J.; Wang, X.; Han, G.; Dai, H. Research on the impact of high-temperature aging on the thermal safety of lithium-ion batteries. *J. Energy Chem.* **2023**, *87*, 378–389. [CrossRef]
17. Zhang, G.; Shen, W.; Wei, X. Lithium-ion battery thermal safety evolution during high-temperature nonlinear aging. *Fuel* **2024**, *362*, 130845. [CrossRef]
18. Shao, D.; Hu, L.; Zhang, J.; Hu, R.; Zhang, G.; Jiang, L.; Wang, X.; Wen, Y. Advanced low-temperature preheating strategies for power lithium-ion batteries applied in electric vehicles: A review. *Int. J. Electrochem. Sci.* **2024**, *19*, 100817. [CrossRef]
19. Ren, X.; Sun, T.; Mao, S.; Zheng, Y.; Han, X.; Ouyang, M. Accelerated aging protocols design for Li-ion batteries based on equivalence of the degradation mechanisms. *J. Energy Storage* **2024**, *99*, 113386. [CrossRef]
20. Wang, M.; Wu, S.; Chen, Y.; Luan, W. The snowball effect in electrochemical degradation and safety evolution of lithium-ion batteries during long-term cycling. *Appl. Energy* **2025**, *378*, 124909. [CrossRef]
21. Guo, Y.; Cai, J.; Liao, Y.; Hu, J.; Zhou, X. Insight into fast charging/discharging aging mechanism and degradation-safety analytics of 18650 lithium-ion batteries. *J. Energy Storage* **2023**, *72*, 108331. [CrossRef]

22. Wang, C.; Tang, Q.; Sun, T.; Feng, X.; Shen, K.; Zheng, Y.; Ouyang, M. Application of high frequency square wave pulsed current on lithium-ion batteries at subzero temperature. *J. Power Sources* **2025**, *633*, 236413. [CrossRef]
23. Wang, R.; Xue, B. Research on aging evolution and safety characteristics of lithium-ion batteries cycling at low temperature. *Batteries* **2025**, *11*, 396. [CrossRef]
24. Zhang, J.; Long, T.; Sun, X.; He, L.; Yang, J.; Wang, J.; Wang, Z.; Huang, Y.; Zhang, L.; Zhang, Y. Mechanism investigation on microstructure degradation and thermal runaway propagation of batteries undergoing high-rate cycling process. *J. Energy Chem.* **2025**, *113*, 1013–1029. [CrossRef]
25. Ni, L.; Tian, J.; Zhang, G.; Zhu, L.; Huang, X.; Lao, L.; Wang, X.; Zhang, H. Mechanism research of temperature and discharge rate effects on sodium-ion battery capacity degradation. *Electrochem. Commun.* **2026**, *187*, 108164. [CrossRef]
26. Zhang, Y.; Ge, X.; Li, X.; Zhao, F.; Zhang, K.; Zhong, W. SOH Prediction of High-Capacity Lithium-Ion Batteries under High-Rate Charging via a TCN-BiGRU Model with Multi-Head Attention. *J. Electrochem. Soc.* **2025**, *172*, 100516. [CrossRef]
27. Zhou, L.; Jin, X.; Chun, E.; Wang, Z.; Liu, J. Thermal behavior and failure mechanisms of lithium-ion battery under high discharging rate. *Appl. Therm. Eng.* **2025**, *278*, 127043. [CrossRef]
28. Huang, Y.; Ruan, Y.; Shen, X.; Zhao, Y.; Li, W.; Shi, Y.; Liu, J.; Wang, J.; Wang, Z. Investigation on thermal runaway characteristics of lithium-ion batteries and barrier inhibition mechanism of aerogel composites under high-rate charge-discharge conditions. *Process Saf. Environ. Prot.* **2026**, *214*, 109024. [CrossRef]
29. Zhang, Z.; Ji, C.; Wang, Y. Failure mechanism and thermal runaway in batteries during micro-overcharge aging at different temperatures. *Materials* **2024**, *17*, 2125. [CrossRef] [PubMed]
30. Guo, D.; Lu, T.; Sun, T.; Lai, X.; Han, X.; Zheng, Y. Facilitating battery quality classification: Early life prediction with sequence-sampling data augmentation. *eTransportation* **2026**, *28*, 100553. [CrossRef]


**Disclaimer/Publisher's Note:** The statements, opinions and data contained in all publications are solely those of the individual author(s) and contributor(s) and not of MDPI and/or the editor(s). MDPI and/or the editor(s) disclaim responsibility for any injury to people or property resulting from any ideas, methods, instructions or products referred to in the content.